Available online at www.sciencedirect.com
SCIENCE DIRECT®
Journal of Sound and Vibration 270 (2004) 495–508
JOURNAL OF SOUND AND VIBRATION
www.elsevier.com/locate/jsvi

Some benchmark problems for computational aeroacoustics

C.J. Chapman*

Department of Mathematics, University of Keele, Keele, Staffordshire ST5 5BG, UK

Accepted 15 September 2003

Abstract

This paper presents analytical results for high-speed leading-edge noise which may be useful for benchmark testing of computational aeroacoustics codes. The source of the noise is a convected gust striking the leading edge of a wing or fan blade at arbitrary subsonic Mach number; the streamwise shape of the gust is top-hat, Gaussian, or sinusoidal, and the cross-stream shape is top-hat, Gaussian, or uniform. Detailed results are given for all nine combinations of shapes; six combinations give three-dimensional sound fields, and three give two-dimensional fields. The gust shapes depend on numerical parameters, such as frequency, rise time, and width, which may be varied arbitrarily in relation to aeroacoustic code parameters, such as time-step, grid size, and artificial viscosity. Hence it is possible to determine values of code parameters suitable for accurate calculation of a given acoustic feature, e.g., the impulsive sound field produced by a gust with sharp edges, or a full three-dimensional acoustic directivity pattern, or a complicated multi-lobed directivity. Another possibility is to check how accurately a code can determine the far acoustic field from nearfield data; a parameter here would be the distance from the leading edge at which the data are taken.

1. Introduction

This paper is concerned with benchmark testing of computer codes which predict the acoustic field generated by a convected gust which strikes the leading edge of a high-speed aerofoil or fan blade. This sound-generation problem, an example of 'blade-vortex interaction,' is of fundamental importance in noise research on turbofan aeroengines and helicopter rotors, and has in recent years attracted much study by the computational aeroacoustics community. The author recently obtained an analytical solution for an idealized version of the problem [1]; the solution, which unifies and generalizes previous work [2–6], gives the full three-dimensional sound

*Tel.: +44-1782-583-262; fax: +44-1782-584-268.
E-mail address: c.j.chapman@maths.keele.ac.uk (C.J. Chapman).

0022-460X/$ - see front matter
doi:10.1016/j.jsv.2003.09.054

field, including the near field, when the gust has arbitrary shape in space and time. Thus the gust may be localized in the span direction of the blade, may be localized in time, and may have sharp edges. The analytical solution is well suited to numerical evaluation; and its farfield approximation is simple enough that for analytically specified gust shapes, e.g., single-frequency, Gaussian, or top-hat, all integrations may be performed analytically. Thus analytical results are available of the way in which the unsteady three-dimensional sound field depends on properties of the incoming gust field, e.g., time-domain features such as sharp edges of the gust, or frequency-domain features described by parameters in a turbulence spectrum; and all results can be converted between the frequency domain (for acoustics) and the time domain (for computational fluid dynamics). Two-dimensional sound fields are also readily obtained from the analytical results. Hence the analysis provides a very large number of exact sound fields which can be used as benchmark checks of computational aeroacoustics codes. Furthermore, the analysis provides a simple transfer function between the incoming gust and the source term in the acoustic part of a code. Our analysis applies to 'non-compact' sound generation at the leading edge, i.e., the frequencies are assumed high enough that the leading edge may be considered separately from the trailing edge. Thus the problem is one of edge diffraction, and the sound field is neither a monopole, dipole, nor quadrupole; the analytical theory shows the field to be half-way between a monopole and a dipole, both in amplitude and directivity. Hence the acoustic field is stronger than a dipole.

Section 2 of this paper gives the analytical solution in its most general form; for the derivation, the reader is referred to Ref. [1]. The solution is used in Section 3 to calculate explicitly some three-dimensional fields, and in Section 4 some two-dimensional fields. Practical considerations in applying the results to computational aeroacoustics codes are discussed in Section 5.

2. Leading-edge noise

2.1. The boundary-value problem for the acoustic field

The system to be investigated is sketched in Fig. 1, which shows part of a flat-plate aerofoil at zero angle of incidence in a uniform free stream of air at speed U. The speed of sound in the air is c_0, and the Mach number of the flow is $M = U/c_0$. The flow is assumed subsonic, i.e., $M < 1$. The

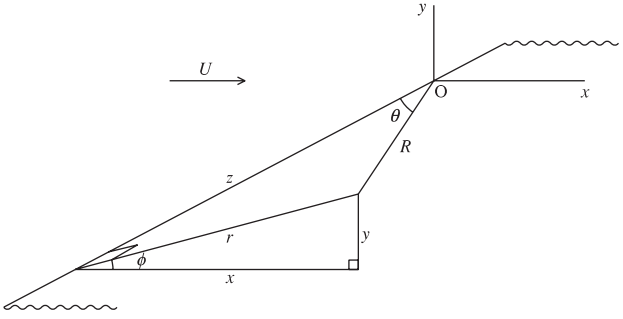

Fig. 1. Flat-plate aerofoil in a uniform flow of speed U; co-ordinate systems are (x, y, z), (r, ϕ, z), and (R, θ, ϕ). The aerofoil occupies the half-plane $y = 0$, $x \geqslant 0$ ($\phi = 0$), and its leading edge is the z-axis ($\theta = 0, \pi$).

axis Ox points along the plate (assumed horizontal) at right angles to the leading edge and in the flow direction; the axis Oy points vertically upwards; and the axis Oz points along the leading edge, horizontally to the right for an observer facing in the positive Ox direction. Corresponding cylindrical co-ordinates are (r, ϕ, z), where r is distance from the leading edge and ϕ is azimuthal angle around the leading edge, measured from the horizontal Oxz plane. The plate occupies the half-plane $\phi = 0$, and the half-plane ahead of the plate is $\phi = \pi$. Corresponding spherical co-ordinates are (R, θ, ϕ), where R is distance from O and θ is polar angle, measured from the leading-edge direction Oz. The positive half $z > 0$ of the leading edge is $\theta = 0$, and the negative half $z < 0$ is $\theta = \pi$.

All final results will be expressed in terms of the aeroacoustic co-ordinates $(\bar{x}, \bar{y}, \bar{z})$ defined by $\bar{x} = x/(1 - M^2)$, $\bar{y} = y/(1 - M^2)^{1/2}$, $\bar{z} = z/(1 - M^2)^{1/2}$. This choice is not unique but leads to formulae with the fewest factors of $(1 - M^2)^{1/2}$; hence $(\bar{x}, \bar{y}, \bar{z})$ appear to be the basic similarity variables for aeroacoustics [7]. Corresponding polar co-ordinates are $(\bar{r}, \bar{\phi}, \bar{z})$ and $(\bar{R}, \bar{\theta}, \bar{\phi})$, defined by

$$(\bar{r}, \tan\bar{\phi}) = ((\bar{x}^2 + \bar{y}^2)^{1/2}, \bar{y}/\bar{x}), \quad (\bar{R}, \tan\bar{\theta}) = ((\bar{r}^2 + \bar{z}^2)^{1/2}, \bar{r}/\bar{z}). \tag{1}$$

All formulae for leading-edge noise depend on $\bar{\phi}$ only through the factor $\cos\frac{1}{2}\bar{\phi}$.

A small-amplitude convected gust is now superimposed on the uniform flow. On inviscid linear theory, the interaction of the gust with the plate occurs only through the vertical component of the gust velocity in the horizontal plane $y = 0$; this component has the functional form $f(t - x/U, z)$. Since the total velocity has zero vertical component on the plate, the boundary-value problem for the acoustic field requires the acoustic velocity on the plate to have vertical component $-f(t - x/U, z)$. Let the undisturbed air have density ρ_0. Then the acoustic velocity $\mathbf{u}$ and the acoustic pressure p may be expressed in terms of a potential $\varphi(t, x, y, z)$ as

$$\mathbf{u} = \nabla\varphi, \quad p = -\rho_0\left(\frac{\partial}{\partial t} + U\frac{\partial}{\partial x}\right)\varphi. \tag{2}$$

Since the plate supports a pressure difference between its upper and lower surfaces, the function φ is discontinuous across the half-plane $y = 0$, $x > 0$. By the symmetry of the problem, φ is odd in y, and hence zero on the half-plane $y = 0$, $x < 0$. With $\mathbf{u} = (u, v, w) = (\varphi_x, \varphi_y, \varphi_z)$ in Cartesian co-ordinates, it follows that u and w are odd in y, and v is even in y. The boundary-value problem for φ, obtainable from linearized thin-aerofoil theory [8], is

$$\frac{1}{c_0^2}\left(\frac{\partial}{\partial t} + U\frac{\partial}{\partial x}\right)^2\varphi - \left(\frac{\partial^2}{\partial x^2} + \frac{\partial^2}{\partial y^2} + \frac{\partial^2}{\partial z^2}\right)\varphi = 0, \tag{3}$$

$$\varphi_y = -f(t - x/U, z) \quad (y = 0^{\pm}, x > 0), \tag{4}$$

$$\varphi = 0 \quad (y = 0, x < 0). \tag{5}$$

In addition, φ must satisfy a radiation condition and a related causality condition, and, in order that the acoustic energy remain finite, be of no higher order than $r^{1/2}$ near the leading edge.

The above derivation of the acoustic boundary-value problem (3)–(5) makes use of the splitting theorem [9, pp. 220–222], which asserts that, for the inviscid linear problem considered here, the total velocity perturbation to the mean flow may be written as the sum of (a) a solenoidal vortical part, linear in fluid-particle velocities, convected with the mean flow and with no associated

pressure perturbation; and (b) a compressible irrotational acoustical part, to which the whole of the pressure perturbation is due. Here (a) is represented by $f(t-x/U,z)$, and (b) is $\nabla\varphi$. The vortical and acoustical parts are uncoupled except through the boundary conditions. The splitting theorem depends on the fact that the mean flow is uniform.

For the boundary-value problem (3)–(5), the sound generated appears to radiate away from the leading edge of the plate, $x=y=0$, rather than from the plate surface. This is the source of the difficulty of the problem for computational aeroacoustics codes. Such codes need exceptionally high accuracy near aerofoil edges (or any other geometrical discontinuity) because the sound generation process takes place on a length scale much smaller than the wavelength of the radiated sound. The underlying difficulty is a disparity in length scales.

2.2. The acoustic field produced by an arbitrary gust

The boundary-value problem (3)–(5) may be solved for φ by taking Fourier transforms in t, x, and z and using the Wiener–Hopf technique. Frequencies will be represented by ω, and wavenumbers conjugate to z by m. The convention for Fourier transforms, represented by capital letters, is

$$F(\omega,m)=\int_{-\infty}^{\infty}\int_{-\infty}^{\infty} f(t,z)\mathrm{e}^{\mathrm{i}(\omega t-mz)}\,\mathrm{d}t\,\mathrm{d}z, \tag{6}$$

$$f(t,z)=\frac{1}{4\pi^2}\int_{-\infty}^{\infty}\int_{-\infty}^{\infty} F(\omega,m)\mathrm{e}^{-\mathrm{i}(\omega t-mz)}\,\mathrm{d}\omega\,\mathrm{d}m. \tag{7}$$

A full derivation of the solution of Eqs. (3)–(5) is given in Ref. [1]; here the results are summarized. The acoustic pressure p is

$$p=\frac{\mathrm{e}^{\pi\mathrm{i}/4}}{4\pi^{5/2}}\frac{\rho_0 c_0 M^{3/2}}{1-M^2}\frac{\cos\frac{1}{2}\bar{\phi}}{\sin^{1/2}\bar{\theta}}\frac{1}{\bar{R}^{1/2}}\int_{-\infty}^{\infty}\left(\frac{\omega}{c_0}\right)^{1/2}\mathrm{e}^{-\mathrm{i}\omega(t+M\bar{x}/c_0)}$$
$$\times\int_C\frac{\mathrm{e}^{\mathrm{i}(\omega\bar{R}/c_0)\cos(\bar{\theta}-\chi)}\sin\chi}{(1+M\sin\chi)^{1/2}}F(\omega,(1-M^2)^{-1/2}(\omega/c_0)\cos\chi)\,\mathrm{d}\chi\,\mathrm{d}\omega. \tag{8}$$

The integration variable χ is a complex angle, and the allowed χ contours C depend on ω. The real part of a complex variable is indicated by a subscript r, and the imaginary part by a subscript i, so that $\chi=\chi_r+\mathrm{i}\chi_i$ and $\omega=\omega_r+\mathrm{i}\omega_i$. When ω is real and positive, one choice of C is the rectilinear path from $\pi-\mathrm{i}\infty$ to $\mathrm{i}\infty$ via π and 0; this path is marked $\mathrm{Q_1Q_2Q_4Q_5}$ in Fig. 2a. When ω is real and negative, the corresponding contour C is from $-\mathrm{i}\infty$ to $\pi+\mathrm{i}\infty$ via 0 and π, and is marked $\mathrm{Q_1'Q_4Q_2Q_5'}$ in Fig. 2b. The contour C may be deformed onto the steepest-descent path through the saddle point of the integrand at $\chi=\bar{\theta}$. In Fig. 2 the steepest-descent path is shown as a dashed line from $\bar{\theta}+\pi/2-\alpha-\mathrm{i}\infty$ to $\bar{\theta}-\pi/2+\alpha+\mathrm{i}\infty$, where α is the phase of ω and $-\pi/2<\alpha<3\pi/2$. Thus the branch line of $\omega^{1/2}$ is taken to run from 0 to $-\mathrm{i}\infty$, indicated by the wavy line in Fig. 3; for causality, the ω contour from $-\infty$ to ∞ in Eq. (8) lies above $\omega=0$, as indicated by contour (i) in Fig. 3, and above any singularities in the ω plane introduced by F. When ω is real and positive, so is $\omega^{1/2}$. The ω contour may be deformed around the branch line, to contour (ii) in Fig. 3, provided that allowance is taken of any poles in F crossed during the deformation.

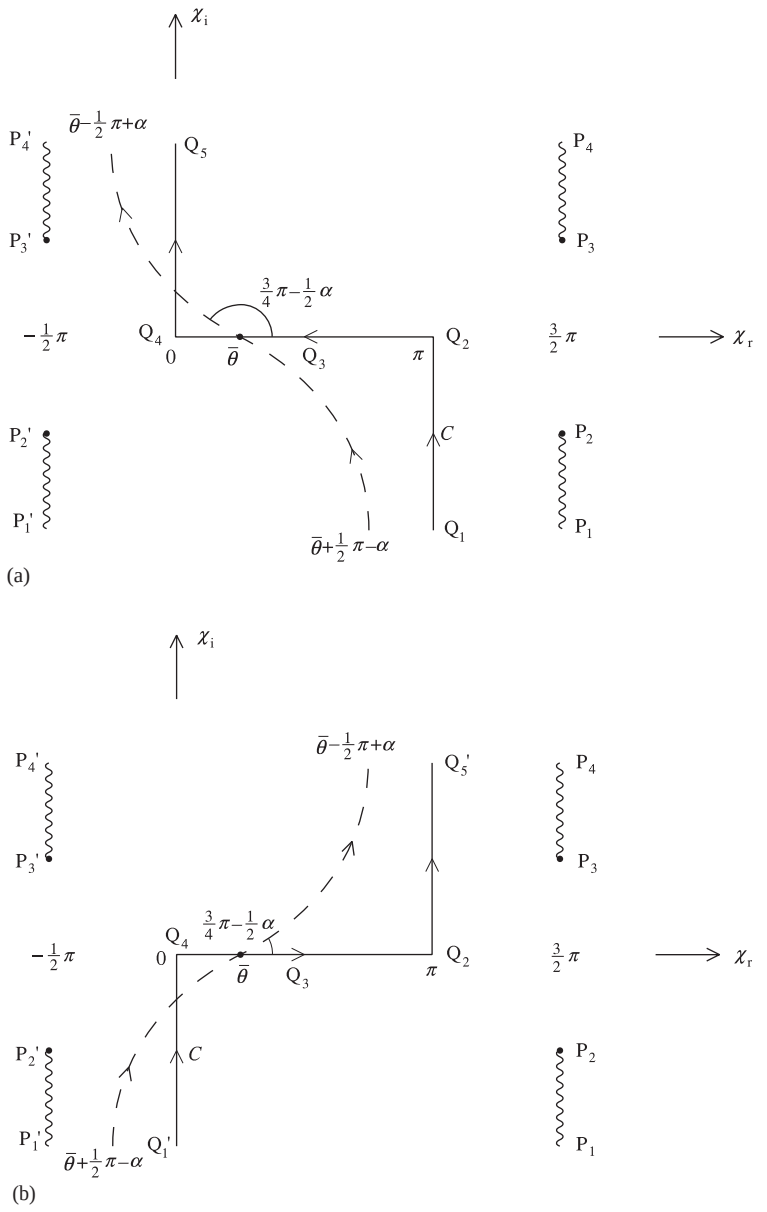

Fig. 2. The χ plane. Wavy lines: branch lines of $(1+M\sin\chi)^{1/2}$, with branch points at P_2, P_3, P_2', P_3'; C: contour for χ integral at fixed ω in (8) when ω is (a) real and positive, and (b) real and negative; dashed line: steepest-descent contour for $\exp\{i(\omega\bar{R}/c_0)\cos(\bar{\theta}-\chi)\}$ when $\omega=\Omega e^{i\alpha}$. The contour is drawn for $\alpha=0$ in (a), and for $\alpha=\pi$ in (b).

The branch points of $(1+M\sin\chi)^{1/2}$ in Eq. (8) are at $\chi=\left(2n-\frac{1}{2}\right)\pi\pm i\cosh^{-1}(1/M)$, $n=0,\pm1,\pm2,\ldots$, from which branch lines may be taken pointing away from the real χ axis, as shown by the points P_3', P_2', P_2, P_3, … and the wavy lines in Fig. 2. The author is concerned only with the 'upper Riemann sheet' of the χ plane, on which $(1+M\sin\chi)^{1/2}$ is real and positive when

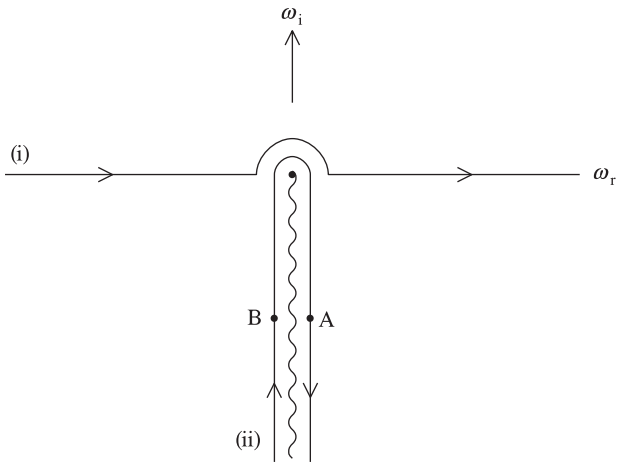

Fig. 3. The ω plane. Wavy line: branch line of $\omega^{1/2}$; (i) contour of ω integral in (8); (ii) deformation of (i) around branch line. With $\omega = \Omega e^{i\alpha}$, points A, B correspond to $\alpha = -\frac{1}{2}\pi, \frac{3}{2}\pi$.

χ is real; recall that it is assumed that $M < 1$. The topology of the Riemann surface in χ is described in Ref. [1].

The ω integration in Eq. (8) may be regarded as performed last. However, if the function F is such that the ω integration can be performed analytically for fixed χ, then the ω integration is conveniently performed first; but account must be taken of the dependence on ω of the χ contour C. This can often be achieved by considering ω real and positive separately from ω real and negative.

If $f(t - x/U, z)$ is real, so that $F(-\omega^*, -m^*) = F^*(\omega, m)$, where the asterisk denotes complex conjugation, then the left and right halves of the ω integral in Eq. (8), including the phase factor $e^{\pi i/4}$, are complex conjugates. The acoustic pressure p is then real, as it must be when f is real; in this case p is twice the real part of the right-hand side of Eq. (8), with the ω contour restricted to its part in the right half of the ω plane.

2.3. The far acoustic field

When $|\omega\bar{R}/c_0| \gg 1$, the dominant contribution to the χ integral in Eq. (8) comes from the neighbourhood of the saddle point $\chi = \bar{\theta}$. Standard theory, given in Ref. [1], shows that a simple farfield approximation to the acoustic pressure, uniform in the polar angle $\bar{\theta}$, is

$$p \sim -\frac{1}{2^{3/2}\pi^2}\frac{\rho_0 c_0 M^{3/2}}{(1-M^2)}\frac{\cos\frac{1}{2}\bar{\phi}\sin^{1/2}\bar{\theta}}{(1+M\sin\bar{\theta})^{1/2}}\frac{1}{\bar{R}}\int_{-\infty}^{\infty} e^{-i\omega(t+M\bar{x}/c_0-\bar{R}/c_0)} \times \left\{1+\frac{iM}{2\sin\bar{\theta}}\frac{c_0}{\omega\bar{R}}\right\}F(\omega,(1-M^2)^{-1/2}(\omega/c_0)\cos\bar{\theta})\,d\omega. \quad (9)$$

Here the integration path in ω is indented above any singularities in F. The second term in braces is needed when $\bar{\theta}$ is close to 0 or π. The physical interpretation of the arguments of F is that, for

given ω and $\bar{\theta}$, the only spanwise wavenumber heard is $m = (1 - M^2)^{-1/2}(\omega/c_0)\cos\bar{\theta}$; this wavenumber corresponds to the oblique sinusoidal gust component with the required trace velocity along the leading edge to produce a ray from the edge to the observer position. The absence of fractional powers of ω in Eq. (9) implies that the three-dimensional sound field produced by a gust which strikes the leading edge for only a limited time does not have a 'tail', i.e., the sound field ends suddenly. In contrast, the near field does have a tail.

The results just stated need to be modified if $F(\omega, (1 - M^2)^{-1/2}(\omega/c_0)\cos\bar{\theta})$ is identically zero for all except isolated values of ω and $\bar{\theta}$. For example, if $f(t - x/U, z)$ does not depend on the span co-ordinate z, then $F(\omega, m)$ contains the factor $\delta(m)$, where δ is the Dirac delta function, and the integrand in Eq. (8) contains the factor $\delta((1 - M^2)^{-1/2}(\omega/c_0)\cos\chi)$, which is zero unless $\omega = 0$ or $\chi = \pi/2$. In this case, the χ integration in Eq. (8) may be performed analytically, to leave an expression containing the factor $(\bar{R}\sin\bar{\theta})^{-1/2}$, i.e., $\bar{r}^{-1/2}$. The physical explanation is that the factor $\bar{R}^{-1}$ in the farfield expression (9) describes spherical spreading of a sound field, in scaled co-ordinates, whereas for a cylindrically spreading sound field, such as that produced by a gust independent of the span co-ordinate, the radial exponent must be $-\frac{1}{2}$. In applications, the form of F in Eq. (8) always leads immediately to the correct radial dependence of the field. A cylindrically spreading sound field obtained from the farfield expression (9) has a tail; thus even if the gust ends suddenly, the sound field does not.

3. Some three-dimensional sound fields

In this section gusts for which the vertical component of velocity is the product of a longitudinal shape function $f_0(t - x/U)$ and a transverse shape function $g(z)$ are considered. Thus in Eq. (4)

$$f(t - x/U, z) = f_0(t - x/U)g(z). \tag{10}$$

Three functions f_0 and two functions g are considered, giving six product functions f. The three longitudinal functions f_0, referred to as single-frequency, Gaussian, and top-hat, are

$$f_0(t - x/U) = v_0 e^{-i\omega_0(t-x/U)}, \quad v_0 e^{-(1/2)\{(t-x/U)/\tau\}^2}, \quad v_0 H((t - x/U)/\tau, -1, 1). \tag{11}$$

Here the parameters are the vertical velocity v_0, the real positive frequency ω_0, and the positive time interval τ. The top-hat function H is defined so that $H(\xi, \xi_0, \xi_1)$ takes the value 1 for $\xi_0 < \xi < \xi_1$ and 0 otherwise. For the Gaussian and top-hat functions f_0, a measure of the streamwise length of the gust is $U\tau$, i.e., $Mc_0\tau$. The two transverse functions g, a Gaussian and a top-hat, are

$$g(z) = e^{-(1/2)(z/a)^2}, \quad H(z/a, -1, 1). \tag{12}$$

Here the parameter a is a positive spanwise length, measuring the width of the gust. Thus the aspect ratio of a gust is $a/(U\tau)$, i.e., $a/(Mc_0\tau)$. The combinations of Eqs. (11) with (12) are referred to as 'single-frequency × Gaussian', etc., with f_0 given first. Now write $\gamma = a^{-1}\int_{-\infty}^{\infty} g(z)\,dz$, so that $\gamma = (2\pi)^{1/2}$ for the Gaussian function $g(z) = e^{-(1/2)(z/a)^2}$, and $\gamma = 2$ for the top-hat function $g(z) = H(z/a, -1, 1)$. The quantity γ is referred to as the transverse shape integral.

The Fourier transform F of Eq. (10) when $x = 0$ is

$$F(\omega, m) = F_0(\omega)G(m), \tag{13}$$

where

$$F_0(\omega) = \int_{-\infty}^{\infty} f_0(t) \mathrm{e}^{\mathrm{i}\omega t}\, \mathrm{d}t, \quad G(m) = \int_{-\infty}^{\infty} g(z) \mathrm{e}^{-\mathrm{i}mz}\, \mathrm{d}z. \tag{14}$$

Thus corresponding to Eqs. (11) and (12)

$$F_0(\omega) = 2\pi v_0 \delta(\omega - \omega_0), \quad (2\pi)^{1/2} v_0 \tau \mathrm{e}^{-(1/2)(\omega\tau)^2}, \quad 2v_0 \omega^{-1} \sin(\omega\tau) \tag{15}$$

and

$$G(m) = (2\pi)^{1/2} a \mathrm{e}^{-(1/2)(ma)^2}, \quad 2m^{-1} \sin(ma). \tag{16}$$

The far acoustic field (9), with the second term in braces neglected and F of the form (13), is

$$p \sim -\frac{1}{2^{3/2}\pi^2} \frac{\rho_0 c_0 M^{3/2}}{1 - M^2} \frac{\cos\frac{1}{2}\bar{\phi} \sin^{1/2}\bar{\theta}}{(1 + M\sin\bar{\theta})^{1/2}} \frac{1}{\bar{R}} \times \int_{-\infty}^{\infty} \mathrm{e}^{-\mathrm{i}\omega(t + M\bar{x}/c_0 - \bar{R}/c_0)} F_0(\omega) G((1 - M^2)^{-1/2}(\omega/c_0)\cos\bar{\theta})\, \mathrm{d}\omega. \tag{17}$$

When the integral is evaluated with F_0 and G given by Eqs. (15) and (16), it is convenient to write the far field in terms of a dimensionless shape factor S defined so that

$$p \sim \rho_0 c_0 \bar{v}_0 M^{3/2} \frac{\cos\frac{1}{2}\bar{\phi} \sin^{1/2}\bar{\theta}}{(1 + M\sin\bar{\theta})^{1/2}} \frac{\bar{a}}{\bar{R}} S. \tag{18}$$

Here $\bar{v}_0 = (1 - M^2)^{-1/2} v_0$ and $\bar{a} = (1 - M^2)^{-1/2} a$, in accordance with the aeroacoustic scaling for lengths transverse to the mean flow. The six far fields are as follows.

3.1. Single-frequency × Gaussian

The vertical component of gust velocity is $v_0 \mathrm{e}^{-\mathrm{i}\omega_0(t - x/U)} \mathrm{e}^{-(1/2)(z/a)^2}$, and the shape factor of the far acoustic field is

$$S = -\pi^{-1/2} \exp\{-\tfrac{1}{2}(\omega_0 \bar{a}/c_0)^2 \cos^2\bar{\theta}\} \mathrm{e}^{-\mathrm{i}\omega_0(t + M\bar{x}/c_0 - \bar{R}/c_0)}. \tag{19}$$

Call the plane $\theta = \frac{1}{2}\pi$ the vertical plane (see Fig. 2). Since $\bar{\theta} = \theta$ when $\theta = 0, \frac{1}{2}\pi, \pi$, it follows that as the observation direction varies from the vertical plane towards the leading edge so $\cos^2\bar{\theta}$ increases from 0 to 1 and the exponential term in Eq. (19) decreases from 1 to $\exp\{-\frac{1}{2}(\omega_0\bar{a}/c_0)^2\}$. Thus if $\omega_0\bar{a}/c_0 \ll 1$, the shape factor S is approximately independent of θ, and from Eq. (18) the dependence of the farfield directivity on θ reduces to $\{(\sin\bar{\theta})/(1 + M\sin\bar{\theta})\}^{1/2}$. If $\omega_0\bar{a}/c_0 \gg 1$, the acoustic field is 'super-directive', being strongly peaked on the vertical plane; the acoustic field then decays exponentially rapidly with angle when $|\cos\bar{\theta}|$ exceeds values of order $(\omega_0\bar{a}/c_0)^{-1}$. Near the vertical plane one may write $\cos\bar{\theta} \simeq -\left(\bar{\theta} - \frac{1}{2}\pi\right)$, so that the exponential factor in Eq. (19) is then approximately $\exp\{-\frac{1}{2}(\omega_0\bar{a}/c_0)^2\left(\bar{\theta} - \frac{1}{2}\pi\right)^2\}$; i.e., in the super-directive regime $\omega_0\bar{a}/c_0 \gg 1$ the acoustic field is effectively confined to $\left|\bar{\theta} - \frac{1}{2}\pi\right| = O((\omega_0\bar{a}/c_0)^{-1})$.

3.2. Single-frequency × top-hat

The vertical component of gust velocity is $v_0 e^{-i\omega_0(t-x/U)} H(z/a,-1,1)$, and the shape factor of the far acoustic field is

$$S = -\frac{2^{1/2}}{\pi}\frac{\sin((\omega_0\bar{a}/c_0)\cos\bar{\theta})}{(\omega_0\bar{a}/c_0)\cos\bar{\theta}}\, e^{-i\omega_0(t+M\bar{x}/c_0-\bar{R}/c_0)}. \tag{20}$$

As the observation direction varies from the vertical plane $\bar{\theta} = \frac{1}{2}\pi$ towards the leading edge $\bar{\theta} = 0, \pi$ the second fraction in Eq. (20) varies from 1 to $\sin(\omega_0\bar{a}/c_0)/(\omega_0\bar{a}/c_0)$. Thus for $\omega_0\bar{a}/c_0 \ll 1$ this fraction is approximately constant at the value 1, whereas for $\omega_0\bar{a}/c_0 \gg 1$ the fraction represents a multi-lobed farfield acoustic directivity pattern, the lobes decaying in amplitude away from the vertical plane. Such a multi-lobed pattern is familiar in high-frequency acoustics (e.g., for a high-frequency oscillating piston in a baffle), where it often occurs as an interference pattern between sound fields produced at the edges of a source region. Here, the shape factor (20) arises from the gust vorticity, which is of delta-function form on the planes $z = \pm a$, and from the fact that sound is produced only at the leading edge of the aerofoil. Thus the sound sources are effectively at the edges of the top-hat on the leading edge, i.e., at $(x, y, z) = (0, 0, \pm a)$.

3.3. Gaussian × Gaussian

The vertical component of gust velocity is $v_0 e^{-(1/2)\{(t-x/U)/\tau\}^2} e^{-(1/2)(z/a)^2}$ and the shape factor of the far acoustic field is

$$S = -\frac{1}{\pi^{1/2}}\{1+(\bar{a}/(c_0\tau))^2\cos^2\bar{\theta}\}^{-1/2}\exp\left\{-\frac{1}{2}\frac{\{(t+M\bar{x}/c_0-\bar{R}/c_0)/\tau\}^2}{1+(\bar{a}/(c_0\tau))^2\cos^2\bar{\theta}}\right\}. \tag{21}$$

As the observation direction varies from the vertical plane $\bar{\theta} = \frac{1}{2}\pi$ towards the leading edge $\bar{\theta} = 0, \pi$ the factor $1+(\bar{a}/(c_0\tau))^2\cos^2\bar{\theta}$ varies from 1 to $1+(\bar{a}/(c_0\tau))^2$. Thus for $\bar{a} \ll c_0\tau$, corresponding to a long thin gust aligned at right angles to the leading edge, the factor is approximately constant at the value 1, whereas for $\bar{a} \gg c_0\tau$, corresponding to a long thin gust aligned parallel to the leading edge, the factor varies considerably, and is approximately $(\bar{a}/(c_0\tau))^2\cos^2\bar{\theta}$ where $|\cos\bar{\theta}|$ exceeds the small value $(\bar{a}/(c_0\tau))^{-1}$, i.e., where $\left|\bar{\theta}-\frac{1}{2}\pi\right|$ is greater than order $(\bar{a}/(c_0\tau))^{-1}$. Hence as in Section 3.2 the far acoustic field depends strongly on the observation angle $\bar{\theta}$ when the length of leading edge 'wetted' by the gust is large, i.e., when there are acoustic sources well separated in space. Although the aspect ratio of the gust is $a/(Mc_0\tau)$, the acoustically important quantity, accounting for the flow, is $\bar{a}/(c_0\tau)$.

For $\bar{a}$ of order at most $c_0\tau$, the factor $-\frac{1}{2}\{(t+M\bar{x}/c_0-\bar{R}/c_0)/\tau\}^2$ in the exponent of Eq. (21) shows that at a fixed observation point the acoustic field is negligible except for a time interval of order τ. The reason is that the gust velocity at the leading edge $x = 0$, being proportional to $e^{-(1/2)(t/\tau)^2}$, provides an acoustic source of significant strength only for a time interval of order τ; the factor gives the effect of this source in terms of the retarded time $t+M\bar{x}/c_0-\bar{R}/c_0$ for acoustic signals in a uniform flow. There is no large-time tail to the significant acoustic field, because the field is spreading spherically. When $\bar{a}$ significantly exceeds $c_0\tau$, the exponent in Eq. (21) shows that the above time interval τ is replaced by $(\bar{a}/c_0)|\cos\bar{\theta}|$, i.e., the time taken for a

signal travelling at speed c_0 to traverse a distance $\bar{a}|\cos\bar{\theta}|$; this is an 'aeroacoustically scaled' version of a familiar result for no mean flow, because $\bar{a}|\cos\bar{\theta}|$ is the scaled length of the projection of the source region onto the radius vector from the source region to the observer.

3.4. Gaussian × top-hat

The vertical component of gust velocity is $v_0 e^{-(1/2)\{(t-x/U)/\tau\}^2} H(z/a,-1,1)$, and the shape factor of the acoustic far field is

$$S = -\frac{1}{\pi^{1/2}} \frac{\{\Phi(T_+) - \Phi(T_-)\}}{(\bar{a}/(c_0\tau))\cos\bar{\theta}}, \tag{22}$$

where

$$T_\pm = (t + M\bar{x}/c_0 - \bar{R}/c_0)/\tau \pm (\bar{a}/(c_0\tau))\cos\bar{\theta} \tag{23}$$

and

$$\Phi(\xi) = \frac{1}{(2\pi)^{1/2}} \int_{-\infty}^{\xi} e^{-(1/2)s^2}\, ds = \frac{1}{2}(1 + \mathrm{erf}(2^{-1/2}\xi)). \tag{24}$$

When $(\bar{a}/(c_0\tau))|\cos\bar{\theta}| \ll 1$, the numerator $\Phi(T_+) - \Phi(T_-)$ of Eq. (22) is approximately $(T_+ - T_-)\Phi'\left(\frac{1}{2}(T_- + T_+)\right)$, where the dash denotes derivative. Since $\Phi'(\xi) = (2\pi)^{-1/2} e^{-(1/2)\xi^2}$, the shape factor becomes $S \simeq -2^{1/2}\pi^{-1} e^{-(1/2)\{(t+M\bar{x}/c_0-\bar{R}/c_0)/\tau\}^2}$. In this limit $(\bar{a}/(c_0\tau))|\cos\bar{\theta}| \ll 1$, the shape factors (21) for the Gaussian × Gaussian gust and Eq. (22) for the Gaussian × top-hat gust may be unified by writing each in terms of the transverse shape integral $\gamma = a^{-1}\int_{-\infty}^{\infty} g(z)\, dz$ introduced after Eq. (12). Each becomes $S \simeq -2^{-1/2}\pi^{-1}\gamma e^{-(1/2)\{(t+M\bar{x}/c_0-\bar{R}/c_0)/\tau\}^2}$. Thus for a gust of small enough spanwise extent, the far acoustic field depends on $g(z)$ through the integral $\int_{-\infty}^{\infty} g(z)\, dz$ rather than through the shape of $g(z)$. For a gust of large spanwise extent, the shape of $g(z)$ makes a difference. This may be checked by comparing Eqs. (21) and (22) for $(\bar{a}/(c_0\tau))|\cos\bar{\theta}| \gg 1$, using where convenient the approximations $\Phi(\xi) \simeq 1 - (2\pi)^{-1/2}\xi^{-1}e^{-(1/2)\xi^2}$ for $\xi \gg 1$ and $\Phi(\xi) \simeq (2\pi)^{-1/2}|\xi|^{-1}e^{-(1/2)\xi^2}$ for $\xi \ll -1$.

3.5. Top-hat × Gaussian

The vertical component of gust velocity is $v_0 H((t - x/U)/\tau, -1, 1)e^{-(1/2)(z/a)^2}$, and the shape factor of the acoustic far field is

$$S = -\pi^{-1/2}\{\Phi(\tilde{T}_+) - \Phi(\tilde{T}_-)\}, \tag{25}$$

where

$$\tilde{T}_\pm = \frac{t + M\bar{x}/c_0 - \bar{R}/c_0 \pm \tau}{(\bar{a}/c_0)|\cos\bar{\theta}|}. \tag{26}$$

The difference $\tilde{T}_+ - \tilde{T}_- = \{(2\bar{a}/(c_0\tau))|\cos\bar{\theta}|\}^{-1}$ is large when $(\bar{a}/(c_0\tau))|\cos\bar{\theta}|$ is small, in contrast to the difference $T_+ - T_-$ in Section 3.4. Thus the acoustic far field produced by a top-hat × Gaussian gust is very different from that produced by a Gaussian × top-hat gust. The reason lies in the different directions of the vortex lines corresponding to the surfaces of discontinuity in the gust velocity field; for the top-hat × Gaussian gust these vortex lines are parallel to the leading

edge of the aerofoil, whereas for the Gaussian × top-hat gust they are parallel to the stream direction. The approximations to $\Phi(\xi)$ given at the end of Section 3.4 show that the shape factor (25) simplifies if either or both of $\tilde{T}_+$ and $\tilde{T}_-$ is large and positive or large and negative; the shape factor also simplifies if $\tilde{T}_+ - \tilde{T}_-$ is not too large, as in the relations for Φ noted after Eq. (24). Since $\tilde{T}_\pm$ changes sign when $t + M\bar{x}/c_0 - \bar{R}/c_0$ passes through $\pm\tau$, the shape factor is a surprisingly complicated function of position. It is simplest to deal separately with the regions of space in which $\bar{R} - M\bar{x} - c_0 t$ is less than $-c_0\tau$, between $-c_0\tau$ and $c_0\tau$, and greater than $c_0\tau$, and for each region, with its corresponding signs of $\tilde{T}_+$ and $\tilde{T}_-$, determine the range of values of $(\bar{a}/(c_0\tau))|\cos\bar{\theta}|$, in relation both to $|(t + M\bar{x}/c_0 - \bar{R}/c_0)/\tau \pm 1|$ and to 1, for which the expression $\Phi(\tilde{T}_+) - \Phi(\tilde{T}_-)$ simplifies. Only a simple limit when $\bar{R} - M\bar{x} - c_0 t$ is between $-c_0\tau$ and $c_0\tau$, and the observation position is close enough to the vertical plane $\bar{\theta} = \frac{1}{2}\pi$ that $(\bar{a}/(c_0\tau))|\cos\bar{\theta}| \ll |(t + M\bar{x}/c_0 - \bar{R}/c_0)/\tau \pm 1|$ will be presented. Then $\tilde{T}_+ \gg 1$ and $\tilde{T}_- \ll -1$, so that $\Phi(\tilde{T}_+) \simeq 1$ and $\Phi(\tilde{T}_-) \ll 1$, whence $S \simeq -\pi^{-1/2}$.

3.6. Top-hat × top-hat

The vertical component of gust velocity is $v_0 H((t - x/U)/\tau, -1, 1)H(z/a, -1, 1)$, and the shape factor of the acoustic far field is

$$S = -\frac{1}{2^{1/2}\pi} \frac{H_0(T_{++})T_{++} - H_0(T_{+-})T_{+-} - H_0(T_{-+})T_{-+} + H_0(T_{--})T_{--}}{(\bar{a}/(c_0\tau))\cos\bar{\theta}}, \tag{27}$$

where

$$T_{\pm\pm} = (t + M\bar{x}/c_0 - \bar{R}/c_0)/\tau \pm 1 \pm (\bar{a}/(c_0\tau))\cos\bar{\theta} \tag{28}$$

and H_0 is the Heaviside step function, defined by $H_0(\xi) = 0$ for $\xi < 0$, and $H_0(\xi) = 1$ for $\xi > 0$. The numerator of Eq. (27) is zero when $T_{\pm\pm}$ are all positive or all negative. Hence the sound field begins and ends suddenly, i.e., does not have a tail. The vortex lines in the gust form horizontal rectangles, of size $2U\tau$ by $2a$, together forming a vertical rectangular tube.

When $\bar{\theta}$ is close to 0 or π, i.e., when the observation point is close to the leading edge, the above formulae need to be modified to take account of the second term in braces in Eq. (9).

4. Some two-dimensional sound fields

Gusts for which the vertical component of velocity is $f_0(t - x/U)$ are now considered. Thus in Eq. (10) we put $g(z) \equiv 1$, so that instead of Eq. (16) $G(m) = 2\pi\delta(m)$, and Eq. (13) becomes $F(\omega, m) = 2\pi F_0(\omega)\delta(m)$. In expression (8) for p, the χ integration may be performed analytically, to give

$$p = -\frac{e^{\pi i/4}}{2\pi^{3/2}} \frac{\rho_0 c_0^{3/2} M^{3/2}}{(1 - M^2)^{1/2}(1 + M)^{1/2}} \frac{\cos\frac{1}{2}\bar{\phi}}{\bar{r}^{1/2}} \int_{-\infty}^{\infty} \omega^{-1/2} e^{-i\omega(t + M\bar{x}/c_0 - \bar{r}/c_0)} F_0(\omega)\, d\omega. \tag{29}$$

The integration path passes above $\omega = 0$ and above any singularities or branch-points in F_0. Eq. (29) is exact within the present linear theory, i.e., is not simply a farfield approximation. By contrast, for the three-dimensional examples considered in Section 3, the χ integration cannot be

performed analytically, and Eq. (8) cannot then be reduced to a single integral except in the far field.

Evaluation of Eq. (29) for the single-frequency, Gaussian, and top-hat gusts (11), with $F_0(\omega)$ as in Eq. (15), gives the following fields.

4.1. Single frequency

The vertical component of gust velocity is $v_0 e^{-i\omega_0(t-x/U)}$ and the pressure field is

$$p = -\frac{e^{\pi i/4}}{\pi^{1/2}} \frac{\rho_0 c_0 \bar{v}_0 M^{3/2}}{(1+M)^{1/2}} (\cos\tfrac{1}{2}\bar{\phi}) \left(\frac{c_0}{\omega_0 \bar{r}}\right)^{1/2} e^{-i\omega_0(t+M\bar{x}/c_0-\bar{r}/c_0)}. \tag{30}$$

This expression, evaluated at $\phi = 0, 2\pi$, gives the standard formula for the loading on a rigid half-plane when struck by a sinusoidal gust.

4.2. Gaussian

The vertical component of gust velocity is $v_0 e^{-(1/2)\{(t-x/U)/\tau\}^2}$, and the pressure field is

$$p = -\frac{1}{2} \frac{\rho_0 c_0 \bar{v}_0 M^{3/2}}{(1+M)^{1/2}} (\cos\tfrac{1}{2}\bar{\phi}) \left(\frac{c_0\tau}{\bar{r}}\right)^{1/2} h(T), \tag{31}$$

where

$$T = (t + M\bar{x}/c_0 - \bar{r}/c_0)/\tau, \tag{32}$$

$$h(T) = |T|^{1/2} e^{-(1/4)T^2} \left\{ I_{-1/4}\left(\tfrac{1}{4}T^2\right) + \mathrm{sgn}(T) I_{1/4}\left(\tfrac{1}{4}T^2\right) \right\}, \tag{33}$$

and $I_{\pm 1/4}$ are modified Bessel functions of order $\pm\frac{1}{4}$. Limiting forms of $h(T)$ are the tail

$$h(T) \sim 2^{3/2} \pi^{-1/2} T^{-1/2} \quad (T \to \infty), \tag{34}$$

the precursor

$$h(T) \sim 2\pi^{-1/2} |T|^{-1/2} e^{-(1/2)T^2} \quad (T \to -\infty), \tag{35}$$

and small-T approximation

$$h(T) = e^{-(1/4)T^2} (2^{1/4} \pi^{-1} \Gamma\left(\tfrac{1}{4}\right) + 2^{3/4} \pi^{-1} \Gamma\left(\tfrac{3}{4}\right) T + O(T^4)) \quad (T \to 0). \tag{36}$$

The inverse square-root tail (34) is typical of a cylindrically spreading wave field. In contrast, a spherically spreading field typically does not have a tail (cf. Section 3.3).

4.3. Top-hat

The vertical component of gust velocity is $v_0 H((t - x/U)/\tau, -1, 1)$, and the pressure field is

$$p = -\frac{2}{\pi} \frac{\rho_0 c_0 \bar{v}_0 M^{3/2}}{(1+M)^{1/2}} (\cos\tfrac{1}{2}\bar{\phi}) \left(\frac{c_0\tau}{\bar{r}}\right)^{1/2} \tilde{h}(T) \tag{37}$$

with T as in (32) and

$$\tilde{h}(T) = \mathrm{H}_0(T+1)|T+1|^{1/2} - \mathrm{H}_0(T-1)|T-1|^{1/2}, \tag{38}$$

where H_0 is the Heaviside step function. Thus $\tilde{h}(T) = 0$ for $T < -1$, and the tail is $\tilde{h}(T) = T^{-1/2} + \frac{1}{8}T^{-5/2} + \cdots$ for $T \gg 1$. Again, this two-dimensional field has an inverse square-root tail.

5. Practical considerations

A desirable feature of a benchmark problem for testing a computer code is that the statement of the problem should contain a rich set of numerical parameters which can be varied in relation to the numerical parameters of the code, e.g., grid size, time step, and amount of artificial viscosity. For a computational aeroacoustic code, the conclusion of a benchmark test would then be that for given grid size, etc., the code can accurately determine the sound generation process and the acoustic directivity in a certain range of wavenumbers and frequencies, and can determine impulsive sound fields up to a certain level of accuracy.

The above consideration has been a primary factor determining the choice of the nine examples of sound fields given in Sections 3 and 4. Thus examples involving delta-functions have not been presented, but instead 'rise-time' or 'width' parameters such as τ and a have been retained. The user of a benchmark test would need to make an informed choice of τ and a, as well as the frequency ω_0, in relation to code parameters. The formulae above contain the non-dimensional parameters $\bar{a}/(c_0\tau)$ and $\omega_0\bar{a}/c_0$, and the non-dimensional variables $\bar{R}/(c_0\tau)$, $\bar{r}/(c_0\tau)$, $\omega_0\bar{R}/c_0$, $\omega_0\bar{r}/c_0$. All formulae contain as a parameter the Mach number M through the similarity variables indicated by the bar notation; the formulae are not restricted to low Mach numbers, only by the requirement $M<1$. The list of nine examples may readily be extended, because the general integrals (8) and (9) are so user-friendly. For example, the discontinuities in the top-hat gust shapes may be smoothed by linear or polynomial ramps of specified rise-time or thickness; the farfield integral (9) can still be evaluated analytically. Thus the formulae offer scope for exploring a large parameter space.

One testable aspect of a code is the determination of the far acoustic field from nearfield data. Section 4 gives two-dimensional fields everywhere in space, including the correct singular behaviour as the leading edge is approached. A cylindrical control surface of arbitrary radius may be placed around the leading edge, and data on this surface used to compute the far field. The accuracy of the computation as a function of control-surface radius is then readily checked. For three-dimensional fields, involving a spherical control surface, the test procedure is similar, except that the exact result for the near field requires numerical evaluation of integral (8). This evaluation is immediate, especially if the χ contour C is deformed onto the steepest-descent path as shown in Fig. 2, since the integrand then decays exponentially with distance from the real χ axis. By varying the gust parameters, far acoustic fields with arbitrarily many lobes in planes containing the leading edge may be obtained, providing tests of arbitrary difficulty for the computer code.

This paper is limited to leading-edge noise; and the aerofoil has been taken to be thin, flat, and at zero angle of incidence. As ever, the price paid for an analytical result is simplified geometry. The benchmark tests made possible by our analytical results may prove useful as 'necessary' checks of computational aeroacoustics codes, even though they cannot be 'sufficient'.

Acknowledgements

The author thanks A.B. Parry and C.L. Morfey for helpful comments.

References

[1] C.J. Chapman, High-speed leading-edge noise, *Proceedings of the Royal Society of London A* 459 (2003) 2131–2151.
[2] R. Martinez, S.E. Widnall, An aeroacoustic model for high-speed unsteady blade-vortex interaction, *American Institute of Aeronautics and Astronautics Journal* 21 (1983) 1225–1231.
[3] R.K. Amiet, Airfoil gust response and the sound produced by airfoil–vortex interaction, *Journal of Sound and Vibration* 107 (1986) 487–506.
[4] M.S. Howe, Contributions to the theory of sound production by vortex-airfoil interaction, with application to vortices with finite axial velocity defect, *Proceedings of the Royal Society of London A* 420 (1988) 157–182.
[5] Y.P. Guo, A note on sound from the interruption of a cylindrical flow by a semi-infinite aerofoil of subsonic speed, *Journal of Sound and Vibration* 128 (1989) 275–286.
[6] S.J. Majumdar, N. Peake, Noise generation by the interaction between ingested turbulence and a rotating fan, *Journal of Fluid Mechanics* 359 (1998) 181–216.
[7] C.J. Chapman, Similarity variables for sound radiation in a uniform flow, *Journal of Sound and Vibration* 233 (2000) 157–164.
[8] C.J. Chapman, *High Speed Flow*, Cambridge University Press, Cambridge, 2000.
[9] M.E. Goldstein, *Aeroacoustics*, McGraw-Hill, New York, 1976.